Atomic-scale compositional structure of InAsP/InP and InNAsP/InP heterostructures grown by molecular-beam epitaxy

S. L. Zuo, W. G. Bi,[a] C. W. Tu, and E. T. Yu[b]
Department of Electrical and Computer Engineering, University of California, San Diego, La Jolla, California 92093-0407

(Received 21 January 1998; accepted 26 May 1998)

Cross-sectional scanning tunneling microscopy (STM) has been used to characterize the atomic-scale structure of $InAs_{0.35}P_{0.65}/InP$ and $InN_{0.01}As_{0.35}P_{0.64}/InP$ strained-layer multiple quantum well structures grown by gas-source molecular-beam epitaxy. Atomically resolved STM images of the (110) cross-sectional plane reveal nanoscale clustering within the $InAs_xP_{1-x}$ alloy layers, with the boundaries between As-rich and P-rich regions in the alloy layers appearing to be preferentially oriented along the [112] and [$\bar{1}$12] directions in the (110) plane. (1$\bar{1}$0) cross-sectional images reveal that considerably less compositional variation appears within the (110) plane; features elongated along the [110] direction are observed, but few ⟨112⟩ boundaries are seen. These observations suggest that the boundaries between As-rich and P-rich clusters may form preferentially within the (111) and ($\bar{1}$11) planes. Comparisons of filled-state images of $InAs_xP_{1-x}/InP$ and $InN_xAs_yP_{1-x-y}/InP$ heterostructures suggest that N incorporation increases the valence-band offset in $InN_xAs_yP_{1-x-y}/InP$ compared to that in $InAs_xP_{1-x}/InP$. © *1998 American Vacuum Society.* [S0734-211X(98)11104-6]

I. INTRODUCTION

The $InAs_xP_{1-x}/InP$ and, more recently, $InN_xAs_yP_{1-x-y}/InP$ heterostructure material systems have shown considerable promise for lasers and other optoelectronic devices operating at 1.06, 1.3, and 1.55 μm.[1–4] For $InAs_xP_{1-x}/InP$ quantum well structures, the compressive strain in the $InAs_xP_{1-x}$ layer leads to a smaller valence-band effective mass that facilitates population inversion in lasers.[5] Furthermore, the large conduction-band offset in this material system[6] ($\Delta E_c \cong 0.75 \Delta E_g$) leads to efficient electron confinement and reduced leakage current in laser diodes, thereby minimizing the threshold current in $InAs_xP_{1-x}/InP$ lasers.[1] Finally, the composition in the $InAs_xP_{1-x}/InP$ system is easier to control than that in the $In_xGa_{1-x}As_yP_{1-y}/InP$ quaternary system, which has been explored extensively for optoelectronic device applications at wavelengths of 0.98–1.55 μm.[2,7] More recently, $InN_xAs_yP_{1-x-y}$ alloys have generated considerable interest, because incorporation of N at low concentration into the $InAs_xP_{1-x}$ alloy layers has been shown to produce a substantial decrease in band gap,[8] can partially compensate for strain due to As present in the alloy, and may possibly increase the conduction-band offset even further.[9] Above room-temperature lasing has been realized in $InN_xAs_yP_{1-x-y}/In_xGa_{1-x}As_yP_{1-y}$ quantum well microdisk lasers, with the improved performance compared to $In_xGa_{1-x}As/In_xGa_{1-x}As_yP_{1-y}$ quantum well lasers possibly due to an enhanced conduction-band offset coming from nitrogen incorporation.[8]

A significant concern in ternary and quaternary III–V semiconductor alloys is the possible presence of ordering, clustering, and/or compositional modulation, phenomena that have been observed to occur in a wide range of III–V material systems[10–12] and that can exert considerable influence on crystal quality, interface quality, and other electronic as well as optoelectronic properties such as band gap,[13] band-edge discontinuities, and transport properties.[14–17] In addition, the $InN_xAs_yP_{1-x-y}/InP$ material system is of considerable interest because the effects of N incorporation on material properties are not clearly understood, but appear to differ considerably from the effects of alloying with other group V elements.[18,19] Detailed characterization and understanding of atomic-scale compositional variations and the effects of N incorporation on compositional structure and band offsets are therefore of great importance for optoelectronic and electronic devices based on these materials.

In this article, we describe scanning tunneling microscope (STM) studies of pseudomorphic $InAs_{0.35}P_{0.65}/InP$ and $InN_{0.01}As_{0.35}P_{0.64}/InP$ multiple quantum well heterostructures grown by gas-source molecular-beam epitaxy (MBE) on (001) InP substrates. Characterization of $InAs_xP_{1-x}/InP$ and $InN_xAs_yP_{1-x-y}/InP$ in these studies has provided detailed information about heterojunction interface properties, nanoscale clustering in $InAs_xP_{1-x}$ alloys, and the qualitative influence of N incorporation on heterojunction band alignments for $InN_xAs_yP_{1-x-y}/InP$.

II. EXPERIMENT

The samples used for these studies were grown by gas-source MBE. A 2500 Å InP buffer layer was grown initially on a (001) n^+ InP substrate, followed by a coherently strained heterostructure consisting of 50 Å $InAs_{0.35}P_{0.65}$ alternating with 100 Å InP for five periods, and then five periods of 50 Å $InN_{0.01}As_{0.35}P_{0.64}$ alternating with 200 Å InP. All epitaxially grown layers were doped n type (n

[a]Present address: Hewlett-Packard Company, 3500 Deer Creek Rd., MS 26M-7, Palo Alto, CA 94304.
[b]Electronic mail: ety@ece.ucsd.edu

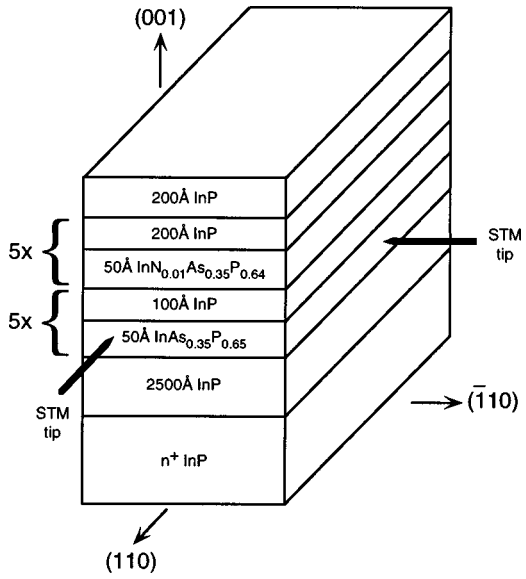

FIG. 1. Schematic diagram of the sample structure and STM geometry used in these studies. STM imaging is performed on both (110) and (110) cross-sectional planes.

$\sim 10^{16}-10^{17}$ cm^{-3}). The substrate temperature during growth was 460 °C; other details concerning the growth chamber and procedures are described elsewhere.[20,21] Figure 1 shows a schematic diagram of the sample structure and STM geometry employed in our work. STM studies were performed on both (110) and (110) cross-sectional surfaces exposed by *in situ* cleaving in an ultrahigh vacuum (UHV) STM chamber at a pressure of $\sim(7-9)\times 10^{-11}$ Torr. Electrochemically etched W tips cleaned *in situ* by electron bombardment were used for these studies.

III. RESULTS AND DISCUSSION

Figure 2(a) shows a 205 Å×205 Å (110) constant-current STM image of the $InAs_xP_{1-x}$/InP multiple quantum well structure, obtained at a sample bias of −2.4 V and a tunneling current of 0.1 nA. Electronically induced contrast between the $InAs_xP_{1-x}$ and InP layers is clearly visible. Because the valence-band edge of InAs is higher than that of InP, we interpret the brighter features as being associated with As and darker features with P within the $InAs_xP_{1-x}$ layer. Variations in composition at the nanometer scale are clearly visible in the $InAs_xP_{1-x}$ alloy layer in Fig. 2(a), allowing us to investigate in detail the nature of clustering in $InAs_xP_{1-x}$. From Fig. 2(a), it is apparent that within the $InAs_xP_{1-x}$ alloy layer there exist brighter As-rich clusters and darker P-rich clusters, as indicated by the arrows. The clustering of As and P within the $InAs_xP_{1-x}$ alloy layers leads to a marked asymmetry in interface quality in the (110) plane—the InP-on-$InAs_xP_{1-x}$ interfaces are considerably rougher and less abrupt than the $InAs_xP_{1-x}$-on-InP interfaces. In Fig. 2(a), dotted lines delineate two As-rich clusters, which appear to possess approximately triangular cross

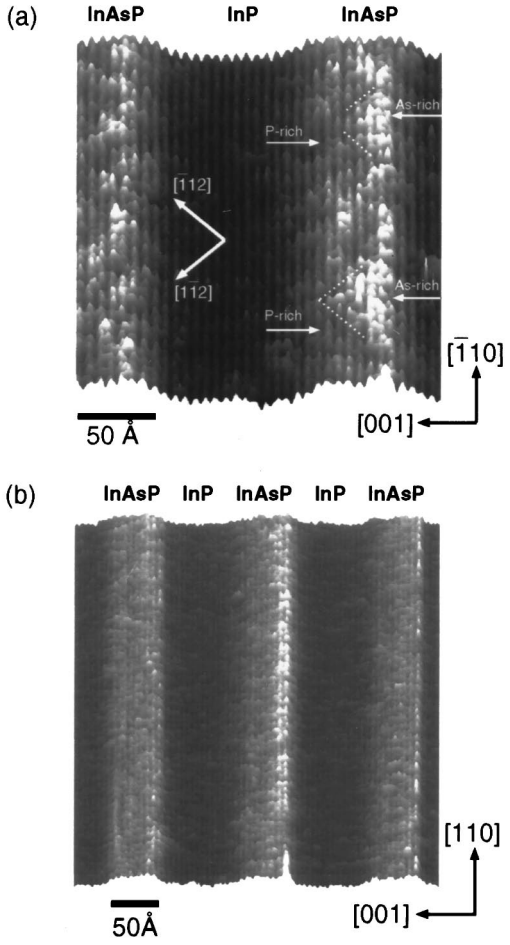

FIG. 2. (a) Three-dimensional rendering of a 205 Å×205 Å (110) constant-current STM image of the $InAs_{0.35}P_{0.65}$/InP multiple quantum well structure, obtained at a sample bias voltage of −2.4 V and a tunneling current of 0.1 nA. Major directions are indicated by arrows. Two triangular As-rich regions, bounded by dotted lines, and two P-rich regions are indicated. (b) Three-dimensional rendering of a 400 Å×400 Å constant-current (110) STM image of the $InAs_{0.35}P_{0.65}$/InP multiple quantum well structure, obtained at a sample bias voltage of −2.4 V and a tunneling current of 0.1 nA.

sections in the (110) plane with bases along the $[\bar{1}10]$ direction and sides appearing to be preferentially oriented along the $[\bar{1}12]$ and [112] directions.

If the boundaries between As-rich and P-rich regions assume the form of simple planes, then the observation that the intersections of the (110) plane and the boundaries between As-rich and P-rich regions within the $InAs_xP_{1-x}$ layers are oriented preferentially along the $[\bar{1}12]$ and [112] directions implies that the boundary plane indices *(hkl)* should satisfy the equation

$$\mp(h-k)+2l=0. \tag{1}$$

The simplest solutions to Eq. (1) correspond to $(\bar{1}11)$ and (111) planes in the crystal, suggesting that the boundaries between As-rich and P-rich regions may form preferentially within these planes.

Imaging of the (110) cross-sectional plane provides further information about the compositional structure present

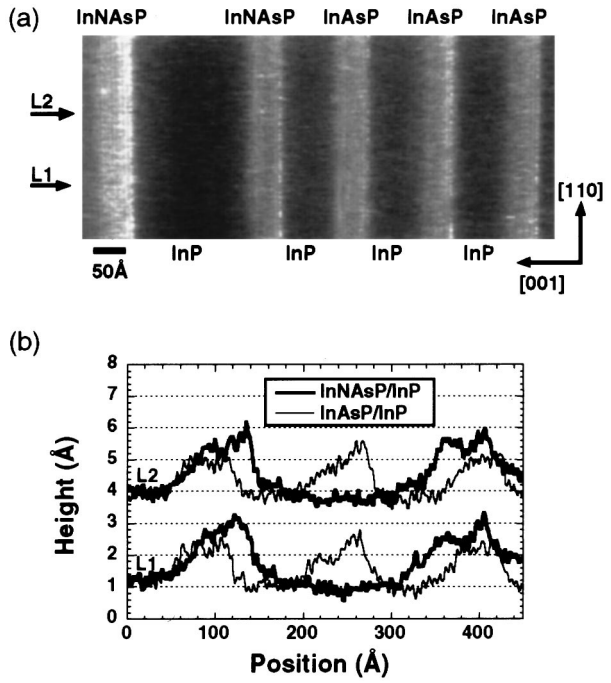

FIG. 3. (a) 860 Å×370 Å constant-current ($1\bar{1}0$) STM image of $InAs_{0.35}P_{0.65}$/InP and $InN_{0.01}As_{0.35}P_{0.64}$/InP multiple quantum well structures, obtained at a sample bias voltage of −2.4 V and a tunneling current of 0.1 nA. (b) Line scans extracted from locations *L1* and *L2* indicated in (a). $InN_{0.01}As_{0.35}P_{0.64}$/InP and $InAs_{0.35}P_{0.65}$/InP profiles are superimposed to compare the topographic contrast observed for each material system.

within the $InAs_xP_{1-x}$ alloy layers. Figure 2(b) shows a 400 Å×400 Å (110) STM image obtained at a sample bias of −2.4 V and a tunneling current of 0.1 nA. In Fig. 2(b), it is apparent that the As composition is graded in the [001] growth direction within the lower two $InAs_xP_{1-x}$ alloy layers: the image contrast is brighter (higher) near the $InAs_xP_{1-x}$-on-InP interfaces and darker (lower) near the InP-on-$InAs_xP_{1-x}$interfaces, corresponding to higher and lower As compositions, respectively. Furthermore, the $InAs_xP_{1-x}$ alloy layers show considerably less compositional variation in the [110] lateral direction than was evident along the [110] lateral direction in the (110) image, and ⟨112⟩ boundaries between clusters are not evident. These observations suggest that the As-rich and P-rich clusters tend to be preferentially elongated in the [110] direction, with approximately triangular cross sections in the (110) plane.

We have also obtained filled-state images of both the $InAs_xP_{1-x}$/InP and the $InN_xAs_yP_{1-x-y}$/InP heterostructures; these images provide information about the effect of N incorporation on the valence-band alignment in these material systems. Figure 3(a) shows a (110) filled-state STM image obtained at a sample bias of −2.4 V and a tunneling current of 0.1 nA. Figure 3(b) shows topographic line scans, each averaged across one atomic spacing, extracted from locations indicated in Fig. 3(a). From the image and the accompanying topographic line profiles, it is apparent that the contrast between the $InN_xAs_yP_{1-x-y}$ and InP layers is greater than that observed between the $InAs_xP_{1-x}$ and InP layers. A direct comparison of topographic contrast between these materials is valid since the comparison is made within the same image and therefore under identical tip and sample conditions. In Fig. 3(b), for each extracted line scan, the contrast between the $InN_xAs_yP_{1-x-y}$and the adjacent InP layer is generally 2 Å or more, while the contrast between $InAs_xP_{1-x}$ and InP layers is usually about 1.5–1.8 Å or less. These observations may indicate that the valence-band offset at the $InN_xAs_yP_{1-x-y}$/InP heterojunction interface is somewhat greater than that for $InAs_xP_{1-x}$/InP.

IV. CONCLUSION

We have performed atomically resolved constant-current cross-sectional STM imaging of $InAs_xP_{1-x}$/InP and $InN_xAs_yP_{1-x-y}$/InP strained-layer multiple quantum well structures grown by gas-source MBE. These studies have revealed the presence of nanoscale clustering of As and P within the $InAs_xP_{1-x}$ alloy layers. A clear asymmetry in interface quality is visible in the (110) plane, with the $InAs_xP_{1-x}$-on-InP interfaces being considerably smoother than the InP-on- $InAs_xP_{1-x}$ interfaces. The boundaries between As-rich and P-rich regions in the $InAs_xP_{1-x}$ alloy layers are oriented preferentially in [112] and [$1\bar{1}2$] directions in (110) images, forming As-rich regions with approximately triangular (110) cross sections. In (110) cross-sectional images, we observe that the As composition in $InAs_xP_{1-x}$ layers varies much less in the lateral direction than in the (110) image. These observations suggest that within the $InAs_xP_{1-x}$ layers, the boundaries between As-rich and P-rich regions may form preferentially within the (111) and ($1\bar{1}1$) planes, and that the As-rich and P-rich clusters tend to be elongated along the [110] direction. Finally, (110) cross-sectional filled-state imaging of both $InAs_xP_{1-x}$/InP and $InN_xAs_yP_{1-x-y}$/InP heterostructures shows that N incorporation into the $InAs_xP_{1-x}$ layer increases the valence-band offset at the $InN_xAs_yP_{1-x-y}$/InP interface compared to that for $InAs_xP_{1-x}$/InP.

ACKNOWLEDGMENTS

Part of this work was supported by DARPA (Optoelectronics Technology Center) and NSF (ECS 95-07986). E.T.Y. would like to acknowledge receipt of a Sloan Research Fellowship.

[1]T. Fukushima, A. Kasukawa, M. Iwase, T. Namegaya, and M. Shibata, IEEE Photonics Technol. Lett. **5**, 117 (1993).
[2]T. K. Woodward, T.-H. Chiu, and T. Sizer II, Appl. Phys. Lett. **60**, 2846 (1992).
[3]H. Q. Hou, A. N. Cheng, H. H. Wieder, W. S. C. Chang, and C. W. Tu, Appl. Phys. Lett. **63**, 1833 (1993).
[4]J. F. Carlin, A. V. Syrbu, C. A. Berseth, J. Behrend, A. Rudra, and E. Kapon, 1997 IEEE 9th International Conference on Indium Phosphide and Related Materials, Cape Cod, MA, 11–15 May, 1997, p. 563.
[5]E. Yablonovitch and E. O. Kane, J. Lightwave Technol. **6**, 1292 (1988).
[6]M. Beaudoin, A. Bensaada, R. Leonelli, P. Desjardins, R. A. Masut, L. Isnard, A. Chennouf, and G. L'Espérance, Phys. Rev. B **53**, 1990 (1996).
[7]H. Q. Hou and C. W. Tu, J. Cryst. Growth **120**, 167 (1992).
[8]W. G. Bi, Y. Ma, J. P. Zhang, L. W. Wang, S. T. Ho, and C. W. Tu, IEEE Photonics Technol. Lett. **9**, 1072 (1997).
[9]L. Bellaiche, S.-H. Wei, and A. Zunger, Phys. Rev. B **54**, 17568 (1996).

[10]H. R. Jen, D. S. Cao, and G. B. Stringfellow, Appl. Phys. Lett. **54**, 1890 (1989).
[11]H. R. Jen, K. Y. Ma, and G. B. Stringfellow, Appl. Phys. Lett. **54**, 1154 (1989).
[12]Y.-E. Ihm, N. Otsuka, J. Klem, and H. Morkoç, Appl. Phys. Lett. **51**, 2013 (1987).
[13]K. A. Mäder and A. Zunger, Appl. Phys. Lett. **64**, 2882 (1994).
[14]G. B. Stringfellow and G. S. Chen, J. Vac. Sci. Technol. B **9**, 2182 (1991).
[15]A. Zunger and S. Mahajan, *Handbook on Semiconductors, Vol. 3B, Materials, Properties and Preparation*, edited by S. Mahajan (North-Holland, Amsterdam, 1994), p. 1399.
[16]P. K. Bhattacharya and J. W. Ku, J. Appl. Phys. **58**, 1410 (1985).
[17]A. Gomyo, T. Suzuki, and S. Iijima, Phys. Rev. Lett. **60**, 2645 (1988).
[18]L. Bellaiche, S.-H. Wei, and A. Zunger, Phys. Rev. B **56**, 10233 (1997).
[19]W. G. Bi and C. W. Tu, Appl. Phys. Lett. **70**, 1608 (1997).
[20]T. P. Chin, B. W. Liang, H. Q. Hou, M. C. Ho, C. E. Chang, and C. W. Tu, Appl. Phys. Lett. **58**, 254 (1991).
[21]H. Q. Hou and C. W. Tu, Appl. Phys. Lett. **60**, 1872 (1992).